Supporting Information

One-Dimensional Multichannel g-$C_3N_{4.7}$ Nanostructure Realizing an Efficient Photocatalytic Hydrogen Evolution Reaction and Theoretical Investigations

Bindu Antil,[§] Lakshya Kumar,[§] Ravi Ranjan,[‡] Sulakshana Shenoy,[ǂ] Kartick Tarafder,[ǂ] Chinnakonda S. Gopinath,[‡] Sasanka Deka*,[§]

[§]Department of Chemistry, University of Delhi, North campus, Delhi-110007, India

[‡]Catalysis and Inorganic Chemistry Division, National Chemical Laboratory, Dr. Homi Bhabha Road, Pune 411 008, India

[ǂ]Department of Physics, National Institute of Technology Karnataka, Srinivasnagar, Mangalore, Karnataka-575025, India

*email: sdeka@chemistry.du.ac.in, ssdeka@gmail.com

Materials. Tetraethyl orthosilicate (TEOS), triethanolamine (TEOA), dicyandiamide ($C_2H_4N_4$), and triblock copolymer poly(ethylene glycol)-block-poly(propylene glycol)-block-poly(ethylene glycol) (pluronic P123, molecular weight = 5800, $EO_{20}PO_{70}EO_{20}$) were obtained from Sigma Aldrich. Hydrochloric acid (HCl, GR grade) was obtained from Molychem.

Synthesis of SBA-15 Template. SBA-15 was prepared by using the same method as reported by Vinu et al.[1] Initially, 4g of the amphiphillic triblock copolymer (P123) was dissolved in 30 ml of DI water and 120 ml of 2M HCl. Afterwards the solution was stirred continuously for 5 h till complete dissolution of the triblock copolymer. Later, 9.6 ml of tetraethylorthosilicate (TEOS) was added drop-wise under constant stirring giving rise to a gel-like suspension. The mixture at this stage was transferred to the hydrothermal vessel and kept for aging at 40 °C for 24 h and then finally heated at 150 °C for 24 h. The product obtained was filtered hot and washed with ethanol carefully. Further, it was dried overnight in oven at 60 °C. The white product obtained was finally calcined in air at 550°C for 6 hours in order to decompose the triblock polymer.

Characterization of the Samples/Instrumental techniques.

The crystalline structures were determined using X-ray diffraction (XRD) technique through a Bruker D8 Advance Diffractometer using monochromatic Cu Kα (λ = 1.54 Å) radiation source. The small angle X-ray scattering (SAXS) measurements were conducted through Xuess SAXS/WAXS system (Model C HP100 fm) equipped with a micro focused sealed tube having Cu anode as X-ray source. The surface area measurements were performed using a Quantachrome (Model ASI-CI-11) BET surface area analyzer, where the sample was degassed for 6h at 150 °C before the adsorption analysis. The Brunauer –Emmett-Teller (BET) method and Barrett-Joyner-Halenda (BJH) method were used to evaluate the specific surface area and pore size values, respectively. The FT-IR spectra were performed in the wavelength range of 400-4000 cm^{-1} employing KBr method using RXI-Mid IR (Perkin Elmer) FT-IR spectrometer. Thermogravimetric measurements were performed under nitrogen atmosphere at a heating rate of 5°/ min to investigate the thermal stability using Mettler Toledo TGA 1 instrument. The morphological characteristics for the as-synthesized samples were studied by Transmission Electron Microscopy (TEM) using Thermo-Scientific Talos Cryo-Transmission Electron Microscope (Cryo-TEM). Similarly, the three dimensional morphological properties and the corresponding elemental composition were investigated by Field Emission Scanning Electron Microscopy (FESEM) using a JEOL JSM 6610 working at 20 kV equipped with Energy Dispersive X-ray spectrometer (EDX). The paramagnetic nature of the material was observed by Electron Paramagnetic Resonance (EPR) measurements using Bruker Model EMX MicroX spectrometer. In order to examine the surface states of the samples and the valence band-edge position, X-ray Photoelectron Spectroscopy (XPS) measurements and XPS valence band measurements were performed using Prevac MX650 XPS system employed with Scienta monochromator (Al Kα anode, 1486.6 eV) and Scienta R3000HP differentially pumped analyzer. C1s peak at 284.4 eV was taken as a reference for all the other binding energies. The stoichiometry of the as-prepared samples were determined by CHN analysis using Elementar Analysensysteme (Model Vario Micro cube, Germany) CHNS analyzer. UV-Vis absorption spectra of the samples taking isopropanol as the reference were recorded using Perkin Elmer LAMDA 35 spectrophotometer. The room temperature photoluminescence (PL) study was conducted on Cary Eclipse Fluorescence spectrophotometer. To examine the lifetime decay of the samples, Time-Resolved Photoluminescence (TRPL) on Horiba Yvon spectrophotometer at an excitation wavelength of 370 nm. Mott Schottky measurements were performed to investigate the absolute conduction band-edge positions relative to normal hydrogen electrode. Prior to deposition of sample ink over glassy carbon electrode (GCE), the sample ink was prepared. The ink was prepared as follows: 10 mg of the MDY sample was dispersed in 1 mL IPA followed by addition of 10 μL of Nafion binder into it, and the resultant mixture was ultrasonicated for 30 mins to obtain a well dispersed sample ink. Flat band edge potential was determined using Dynamic impedance method.

Photoelectrochemical Measurements: The transient photocurrent response (TPC) plots and electrochemical impedance spectroscopy (EIS) measurements were conducted on CHI660E, USA at room temperature using a standard three-electrode system where a Pt wire and Ag/AgCl (saturated KCl) were used as counter and reference electrodes respectively. FTO electrode coated with carbon nitride sample was employed as the working electrode. The preparation of the working electrodes were done as follows: 10 mg of the samples (MDY, BDY) were dispersed in 0.5 ml DMF and 20 μL of Nafion binder through sonication for 30 min. About, 100μL of this ink were spread onto FTO-coated glass slides (1 x 1 cm^2). The films were dried at 60˚C for 1 hour and then annealed at 200˚C for 2 hours for better adhesion. The electrodes were immersed in an aqueous solution containing 0.5 M Na_2SO_4 (inert electrolyte). Transient photocurrent responses were obtained under on/off illumination cycles at constant bias voltage of -0.2 V vs Ag/AgCl. Before the irradiation (dark), current equilibrium was achieved at applied bias voltage. The interval of light-on and light-off was 30 s.

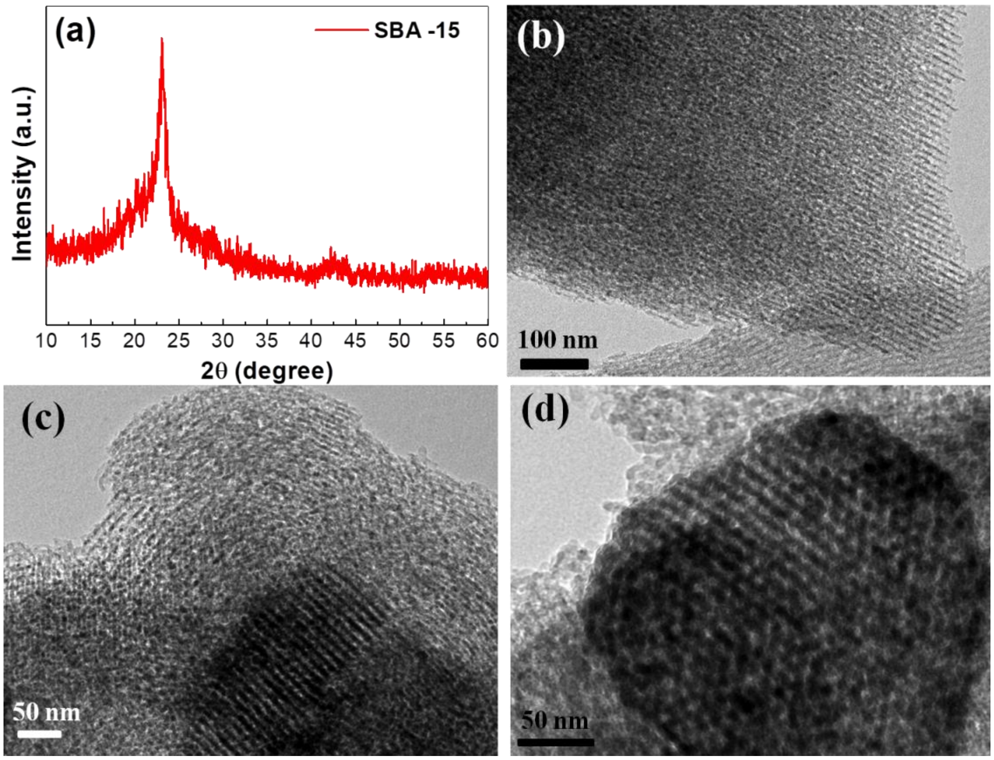

Figure S1. (a) Powder XRD pattern of SBA-15 template in the 2θ range from 0˚ to 5˚. (Inset: Corresponding wide-angle XRD pattern). (b) Low-resolution transmission electron microscopy (TEM) image of SBA-15 template showing the mesoporous structure. (c) High-resolution TEM image illustrating the regular arrangement of pores. (d) High-resolution TEM image of the SBA-15 template.

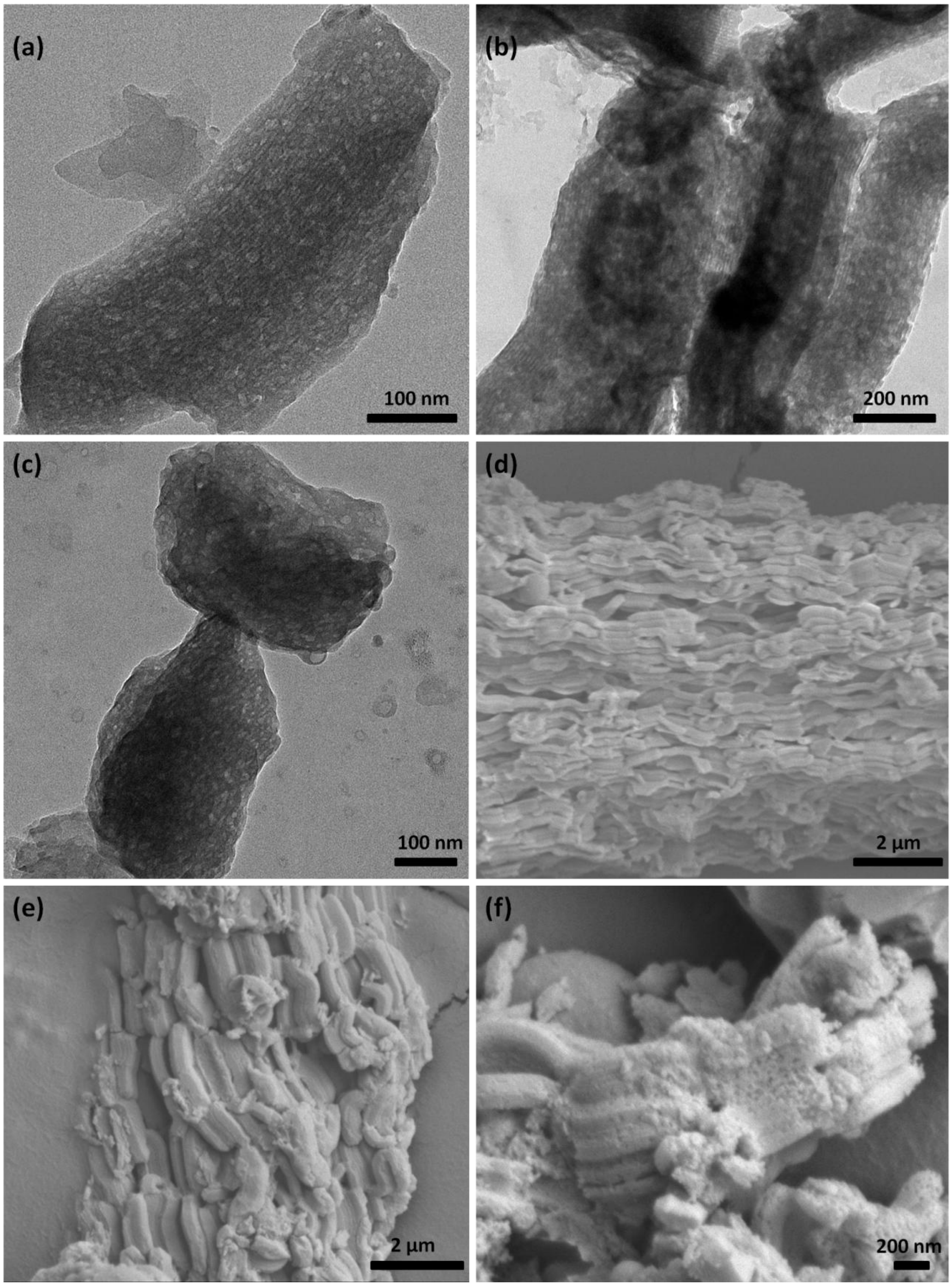

Figure S2. (a-c) TEM images of MDY sample exhibiting hexagonally ordered rope-like mesoporous structure. (d-f) FESEM images of MDY sample showing rope-like structure of MDY sample.

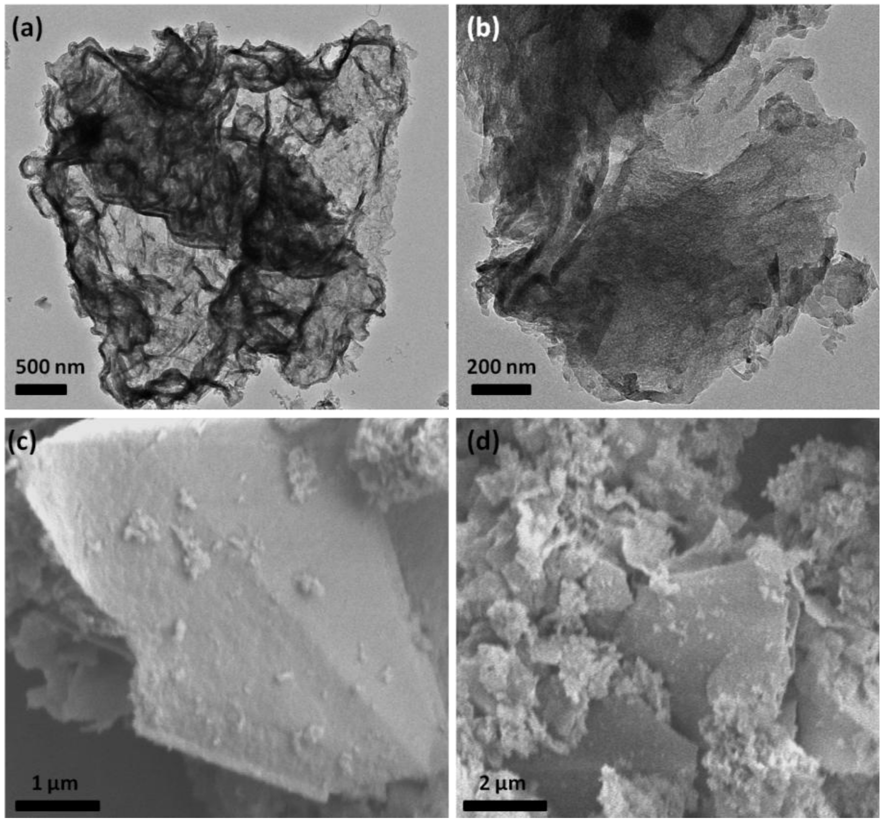

Figure S3. (a-b) TEM images of BDY sample showing sheet-kind of morphology with no observable porosity. (c-d) FESEM images of the BDY sample.

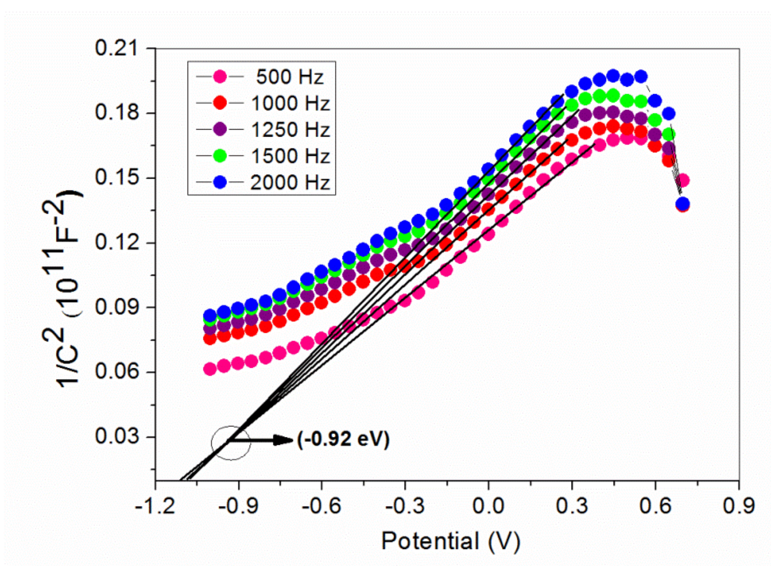

Figure S4. Mott-Schottky measurements of BDY sample.

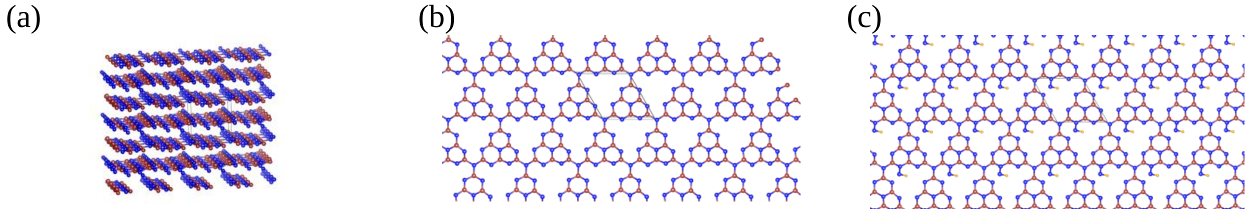

Figure S5. Optimized geometric structure of (a) bulk g-C_3N_4, (b) mono layer of g-C_3N_4 and (c) mono-layer of g-$C_3N_{4.7}$.

Table S1. Depiction of structural parameters of Mesoporous carbon nitride (MDY) and SBA-15 obtained using nanocasting technique.

Sample	**S_{BET} (m^2g^{-1})**	**Pore volume ^{a}(cm^3 g^{-1})**	**Pore size^b (nm)**	**Pore size from TEM (nm)**	**d_{100}^{c} (nm)**	**a_o^{d} (nm)**	**wall thickness^e (nm)**
SBA-15	305	0.31	6.9	7.0	5.9	20.43	2.47
MDY	220	0.72	6.2	6.2	5.5	19.02	1.05
BDY	23.5	0.079	0.13				

^{a}Evaluated at P/P_o= 0.99, where P is the equilibrium pressure and P_o is the saturation pressure of nitrogen at 77K. ^{b}Determined using BJH method from the centre of the pore size distribution curve obtained from the adsorption branch. ^{c}d (100) spacing of the characteristic reflection.

^{d}Calculated using the equation[2] $a_o = 2d_{100}\sqrt{3}$. S1

^{e}Determined using the following equations: $w_d = c\, d \left(\frac{\rho V_p}{1+\rho V_p}\right)^{1/2}$ S2

where:
w_d is the primary mesopore diameter.
d is the XRD (100) reflection plane spacing.
c is a constant characteristic of the pore geometry and equals to 1.213 for circular as well as hexagonal pores.
ρ is pore wall density and assumed to be 2.2 cm^3 g^{-1}

The pore wall thickness $\boldsymbol{b_d}$ is determined further using the equation:

$$\boldsymbol{b_d} = \left(\frac{2}{\sqrt{3}}\right) d_{100} - \frac{w_d}{1.050} \qquad \text{S3}$$

Table S2. Analyzation of Structural parameters of Mesoporous carbon nitride (MDY) obtained with earlier reports.

SI. No.	**Mesoporous carbon nitride materials**	**Measured Surface Area (m^2g^{-1})**	**Pore Volume ($cm^3\ g^{-1}$)**	**Mesopores size (nm)**	**References**
1.	**MDY**	**220**	**0.72**	**6.2**	**This work**
2.	Mesoporous g-C_3N_4 nanorods	100-200	-	3.9	3
3.	Uniformly graphitic carbon nitride	52	-	-	4
4.	Tubular g-C_3N_4	130		macroporous	5
5.	Nanoporous g-C_3N_4	135.1	1.39	60	6
6.	Porous-g C_3N_4	239.17	0.59	4.89	7
7.	N-rich mesoporous carbon nitride	298	0.66	5.8	8

Table S3. Corresponding CHN analysis of MDY sample to analyze the elemental composition.

Sample code	**C [%]**	**N [%]**	**H [%]**	**C/N ratio**	**Stoichiometry**
MDY	30.18	55.01	2.129	0.64	**$C_3N_{4.7}$**

Table S4. CHN analysis of conventional bulk carbon nitride samples prepared following literature methods and comparison with present as-synthesized samples (MDY and BDY).

Sl. No.	Sample code	C [%]	N [%]	H [%]	C/N ratio	Stoichiometry	References followed for synthesis
1	MDY	30.18	55.01	2.129	0.64	**$C_3N_{4.7}$**	**This work**
2	BDY	34.96	55.70	2.041	0.73	**$C_3N_{4.0}$**	**This work**
3	GC-1	35.77	58.23	2.113	0.72	$C_3N_{4.1}$	9
4	GC-2	35.36	56.82	2.097	0.73	$C_3N_{4.0}$	10
5	GC-3	36.28	58.11	1.733	0.73	$C_3N_{4.0}$	11
6	GC-4	35.07	56.77	2.052	0.72	$C_3N_{4.1}$	12
7	GC-5	35.16	55.76	1.932	0.73	$C_3N_{4.0}$	13

<u>Calculations of average lifetime:</u>

The average lifetime (τ_a) can be determined using the following equation:

$$\tau_a = \frac{A_1\tau_1^2+A_2\tau_2^2+A_3\tau_3^2}{A_1\tau_1+A_2\tau_2+A_3\tau_3} \quad \text{S4}$$

where τ_1, τ_2 and τ_3 are lifetime components and A_1, A_2 and A_3 are the amplitudes of the components, respectively.

Table S5. The decay lifetimes and the average lifetime of photoexcited charge carriers in BDY and MDY photocatalysts are listed below:

Sample	Decay life time (ns)			Avg. life time (ns)
	τ_1	τ_2	τ_3	
BDY	0.23	1.61	11.6	**7.16**
MDY	3.42	0.61	18.4	**11.74**

Table S6. The corresponding measured pH values of different SRs used in the photocatalytic reaction.

SI. No.	Sacrificial Agent (SRs)	Measured pH
1.	Water	7
2.	10 % MeOH	9.07
3.	10 % Lactic Acid	1.87
4.	10 % TEOA	10.6
5.	20 % TEOA	10.9

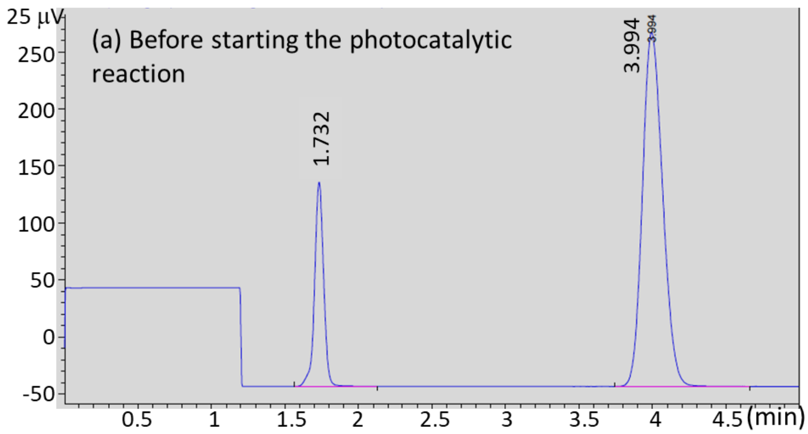

Peak	Ret. Time	Area	Height	Area %/unit
1	1.732	762	179	20.41
2	3.994	2971	310	79.59
Total		3733	489	100.00

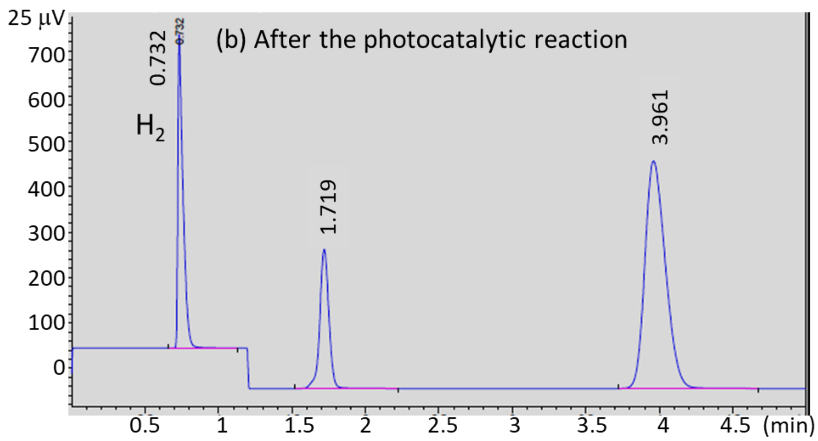

Peak	Ret. Time	Area	Height	Area %/unit
1	0.732	1690	691	21.51
2	1.719	1313	307	16.71
3	3.961	4855	501	61.78
Total		7858	1499	100.00

Figure S6. GC data (a) sample collected before starting the photocatalytic reaction and (b) sample collected after 3 hour of the photocatalytic reaction.

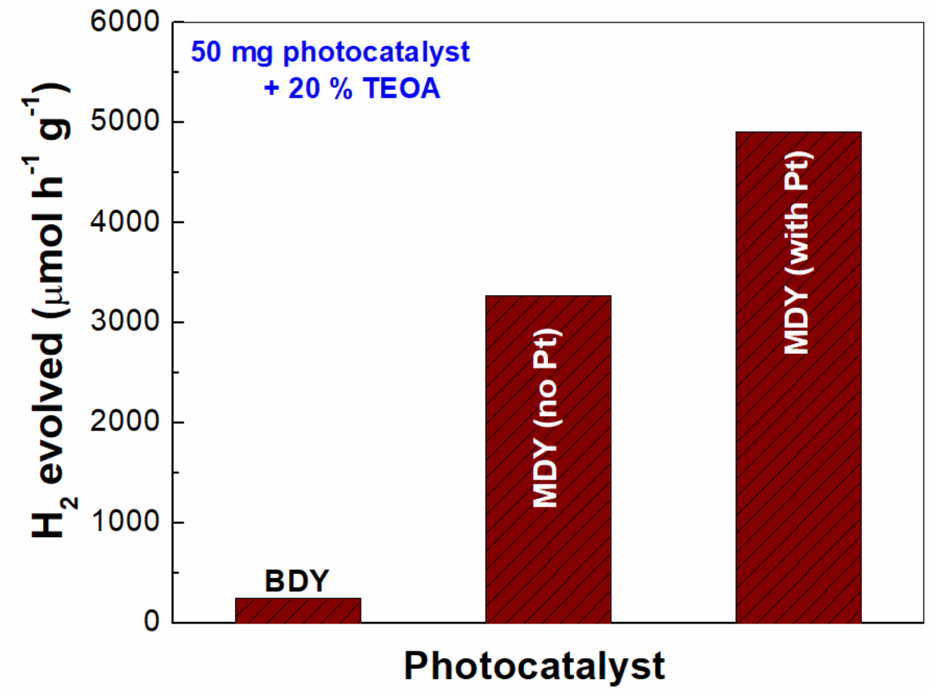

Figure S7. Amount of H_2 evolved per hour per gram of the studied MDY sample in absence and presence of Pt cocatalyst.

Calculations:

Determination of Donor Concentration (N_A) of MDY sample using slope from Mott-Schottky plot.

$$slope = 2/(\varepsilon_o\, \varepsilon_r\, q\, N_A) \qquad \text{S5}$$

ε_o = permittivity of vacuum

ε_r = permittivity of vacuum

q = electron charge

N_A = donor concentration of MDY sample

Therefore, $N_A = 2/\ 8.85 \times 10^{-10} * 9.58 * 1.602 \times 10^{-19} * 3.45 \times 10^{9}$

$= \mathbf{4.26 \times 10^{17}\ cm^{3}}$

Photocatalytic Reaction

1. **Number of H_2 molecule produced from MDY using 3 wt% Pt**

Volume of gas liberated in reaction = 6.0 ml = 0.006 L

Form std. gas equation **PV= nRT**

$n = 0.006\ L \times 1\ atm / 0.082\ L.atm\ mol^{-1}\ K^{-1} \times 298\ K$

The corresponding amount of hydrogen in moles = 0.000245 moles h^{-1}

1 mole gas = 6.023×10^{23} molecules

0.000245 moles will have = $6.023 \times 10^{23} \times 0.000245$

H_2 molecule (*per cm² per s*) = $(6.023 \times 10^{23} \times 0.000245) / (31.4 \times 60\ min \times 60\ s)$

= $\mathbf{1.307 \times 10^{15}}$

H_2 molecule (*per s*) = $(6.023 \times 10^{23} \times 0.000245) / (60\ min \times 60\ s)$

= $\mathbf{4.09 \times 10^{16}}$

2. **Number of H_2 molecule produced from MDY (no Pt)**

Volume of gas liberated in reaction = 4 ml = 0.004 L

Form std. gas equation **PV= nRT**

$n = 0.004\ L \times 1\ atm / 0.082\ L.atm\ mol^{-1}\ K^{-1} \times 298\ K$

The corresponding amount of hydrogen in moles = 0.0001635 moles h^{-1}

1 mole gas = 6.023×10^{23} molecules

0.0001635 moles will have = $6.023 \times 10^{23} \times 0.0001635$

H_2 molecule (*per cm² per s*) = $(6.023 \times 10^{23} \times 0.0001635) / (31.4 \times 60\ min \times 60\ s)$

= $\mathbf{8.71 \times 10^{14}}$

H_2 molecule (*per s*) = $(6.023 \times 10^{23} \times 0.0001635) / (60\ min \times 60\ s)$

= $\mathbf{2.73 \times 10^{16}}$

3. **For Bulk sample (BDY)**

Volume of gas liberated in reaction = 0.3 ml = 0.0003 L

Form std. gas equation **PV= nRT**

$n = 0.0003\ L \times 1\ atm / 0.082\ L.atm\ mol^{-1}\ K^{-1} \times 298\ K$

The corresponding amount of hydrogen in moles = 0.0000163 moles h^{-1}

1 mole gas = 6.023×10^{23} molecules

0.0000163 moles will have = $6.023 \times 10^{23} \times 0.0000163$

H_2 molecule (*per cm^2 per s*) = (6.023 x 10^{23} x 0.0000163) / (31.4 x 60 min x 60 s)

= **8.7 x 10^{13}**

H_2 molecule (*per s*) = **2.72 x 10^{15}**

Apparent quantum Yield (AQY):

$$AQY = \frac{2.nH_2}{number\ of\ incident\ photons}\ x\ 100\ (\%)$$

$$AQY = \frac{2.nH_2}{(IA\lambda)/(hc)}\ x\ 100\ (\%) \qquad \text{S6}$$

Where nH_2 is the number of H_2 molecule produced per second, I is the incident solar irradiance (W/cm^2) over the irradiated area A (cm^2), λ is the wavelength of the present study (nm), h Planck's constant and c is the speed of light.

I = 52500 lux = 0.00768 W/cm^2

A = 31.41 cm^2

1 photon = $\frac{hc}{\lambda}$ =6.626 x10^{-34} x 3 x10^{8} / (λ x 10^{-9})

$$AQY = \frac{2\ x\ nH_2}{(0.00768\ x\ 31.41\ x\ \boldsymbol{\lambda}\ x\ 10^{-9})/(6.626\ x\ 10^{-34}\ x\ 3\ x\ 10^{8})}\left(\frac{s^{-1}}{(\frac{W}{cm2}.cm2.m)/(J.s.m.s^{-1})}\right) x\ 100\%$$

Table S7. The apparent quantum yield of BDY and MDY samples calculated at all wavelengths (5/10 nm intervals) till 420 nm from band gap absorption:

SI. N.	Wavelength (λ value in above equation S5)	AQY (%) (bulk BDY)	AQY (%) of MDY
1.	420	1.06	16.04
2.	425		15.86
3.	430	1.04	15.67
4.	435		15.49
5.	440	1.01	15.31
6.	445		15.14
7.	450	0.99	14.97
8.	455		14.81
9.	460	0.97	14.65
10.	465		14.49

11.	470	0.95	14.34
12.	475		14.19
13.	479	0.93	14.07

Table S8. Comparison of photocatalytic activity of present vermicular rope like mesoporous sample with other nanostructured mesoporous g-C_3N_4 samples and other related photocatalysts.

Sl. No.	Photocatalyst	Amount of photocatalyst and Pt	Sacrificial agent	Photocatalytic Activity (mmol h^{-1} g^{-1})	Apparent Quantum Efficiency (%)	Reference No.
1.	**Mesoporous g-$C_3N_{4.7}$**	**50 mg + 3 wt % Pt**	**20 % vol TEOA**	**4.19**	**16.04 % at 420 nm**	**This work**
		50 mg + without Pt		**3.13**	**10.71 % at 420 nm**	
2.	Mesoporous carbon nitride	100 mg +3 wt % Pt	10% vol TEOA	0.3	0.21 % at 405 nm	14
3.	Mesoporous carbon nitride	30 mg + 3wt % Pt	10% vol TEOA	1.16	7.7% at 420 nm	15
4.	Rh_xP/g-C_3N_4	50 mg	20% vol TEOA	3.055	18.4 % at 420 nm	16
5.	Holey graphitic carbon nitride nanotubes	20 mg + 0.5 wt% Pt	20% Lactic acid	1.07	-	17
6.	Pt@Au NRs/C_3N_4 nanotubes	20 mg catalyst + 3wt % Pt	10 % TEOA	10.35	9.1 % at 420 nm	18
7.	2D FeS-FeS_2	30 mg	0.35 M Na_2SO_3+0.15 Na_2S	2.07	-	19
8.	P-doped g-C_3N_4 nanosheets	50 mg + 1 wt% Pt	10% TEOA	2.61	7.7% at 420 nm	20
9.	Ni_2P/ g-C_3N_4	50 mg +Ni_2P	10% TEOA	2.84	18.8% at 420 nm	21
10.	1T PtS_2/MCN	50 mg + 1 wt% PtS_2	10% TEOA	0.29	1.16% at 405 nm	22
11.	MCN-8	100 mg + 3wt % Pt	10% vol TEOA	2.6	–	23

12.	CoNi-$ZnIn_2S_4$	30 mg	0.1 M ascorbic acid	3.336	-	24
13.	COP-TF@CNi_2P	9 mg	Na_2S + Na_2SO_3	2.5	1.4 % at 500 nm	25
14.	g-C_3N_4/Co@NC	10 mg +1 wt% Pt	15% TEOA	1.56	6.85 at 420 nm	26
15.	Ni-single atom/CN	25 mg + 0.2 at% Ni	10 % TEOA	0.35	-	27
16.	PtSn-CN_x	100 mg + PtSn	20% TEOA	2.96	8.42% at 435 nm	28
17.	Nitrogen vacancies into crystalline g-CN	50 mg + 2 wt% Pd	10 % MeOH	0.55	-	29

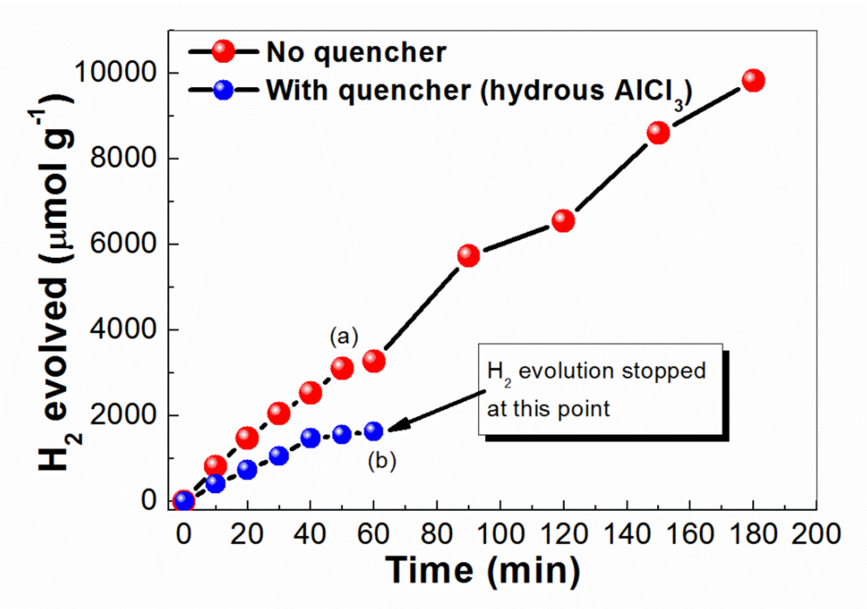

Figure S8. Prolonged 3 h continuous study of photocatalytic hydrogen evolution study using MDY (a) without radical scavenger, and (b) with scavenger (hydrous $AlCl_3$).

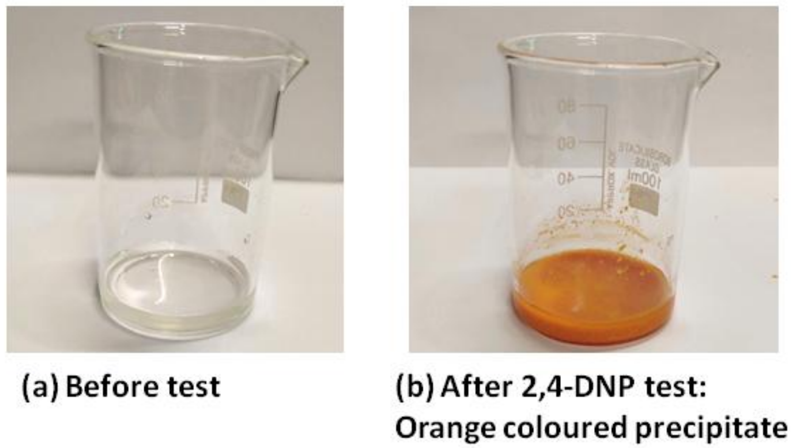

Figure S9. 2,4-dinitrophenylhydrazine (2,4-DNP) test to detect the formation of aldehyde. (a) Solution left out after photocatalytic H_2 evolution reaction and before the addition of 2,4-DNP reagent, (b) Same solution after the addition of 2,4-DNP reagent.

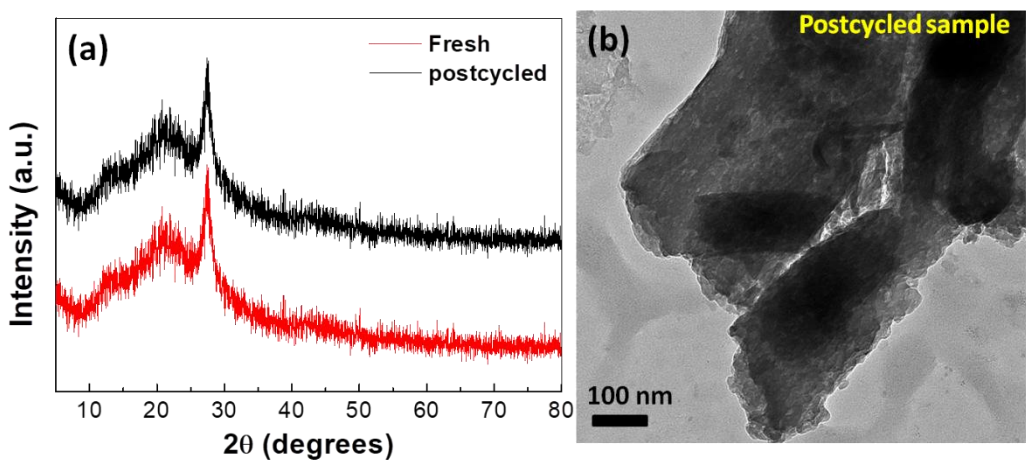

Figure S10. (a) Comparison of powder XRD patterns of fresh MDY sample and post catalytic MDY sample. (b) HRTEM images of the post-catalytic MDY sample.

Table S9. Comparison of efficacy of the present material in this work with the recent g-C_3N_4 and similar co-catalyst with a similar reactor configuration (50 ml).

SI. No.	Photocatalyst	Amount of photocatalyst and Pt in 50 ml reactor	Sacrificial Agent	Photocatalytic activity (mmolh^{-1}g^{-1})	Apparent Quantum Efficiency (%) at 420 nm	Reference No.
1.	**Mesoprous g-$C_3N_{4.7}$**	**50 mg + 3 wt % Pt**	**20 % vol TEOA**	**4.19**	**16.04 % at 420 nm**	**This work**
2.	Fish-scale structured g-C_3N_4	50 mg +3 wt% Pt	10 vol% TEOA	1.316	-	30
3.	g-C_3N_4	50 mg +3 wt% Pt	10 vol% TEOA	0.162	1.4	31
4.	g-C_3N_4 nanostructure	50 mg +3 wt% Pt	10 vol% TEOA	3.135	21.03	32
5.	Holey graphitic carbon nitride	50 mg +3 wt% Pt in 40 ml reactor	10.7 vol% TEOA	8.290	-	33
6.	3D Ordered close-packed g-C_3N_4 nanosphere arrays	50 mg +3 wt% Pt	10 vol% TEOA	3.138	5.07	34
7.	g-C_3N_4	50 mg +1 wt% Pt	10 vol% TEOA	2.7	-	35
8.	g-C_3N_4	50 mg +3 wt% Ni	10 vol% TEOA	0.11	2.6	36
9.	Porous oxygen doped g-C_3N_4	50 mg +3 wt% Pt	20 vol% TEOA	0.395	0.79	37
10.	Carbon-rich g-C_3N_4 nanosheets	50 mg +3 wt% Pt	12 vol% TEOA	0.792	4.52	38
11.	Nanoporous g-C_3N_4	25 mg + 0.5 wt% Pt	10 vol% TEOA	0.008	-	39

POSCAR for g-C_3N_4

```
g-C3N4_heptazine_Phase_1
   1.00000000000000
     6.8685919899354158    0.0062264310321799    0.0000000000000000
    -3.4070984882571040    5.9639982045349234    0.0000000000000000
     0.0000000000000000    0.0000000000000000   10.0000000000000000
   C    N
     6     8
Direct
  0.9061677315109549  0.4158392555043307  0.2558324363580269
  0.5841608585378850  0.0938324169186089  0.3544354636419698
  0.2578923492893139  0.0945748645039401  0.3302903630821206
  0.9054249980273639  0.7421076104179605  0.2799775369178832
  0.9034806221731628  0.0965193691825377  0.3051340000000025
  0.5703011148300945  0.4296989971626743  0.3051340000000025
  0.3615030873623795  0.9801336808943262  0.3674864253266819
  0.0198663928244898  0.6384969911753444  0.2427814746733148
  0.9914881088844112  0.2812090883151868  0.2295154296835022
  0.7187908965370866  0.0085119032234644  0.3807524703164944
  0.6836034041766226  0.6497174564631223  0.2897546079783169
  0.3502825971908337  0.3163967104806531  0.3205132920216798
  0.0254067521785544  0.9745932353746269  0.3051340000000025
  0.6875985365856536  0.3124015722939077  0.3051340000000025
```

POSCAR for g-$C_3N_{4.7}$

```
super cell
   1.00000000000000
     9.5800000000000001    0.0000000000000000    0.0000000000000000
    -4.7900000000000000    8.2965239999999998    0.0000000000000000
     0.0000000000000000    0.0000000000000000   12.0000000000000000
   C    N    H
    12    19     3
Direct
  0.0923756571197032  0.3398857599075598  0.4279012586418034
  0.6151942879454211  0.2855129802149463  0.3236202433205690
  0.1490556245946664  0.7891275868695331  0.3778813118019642
  0.6414617062374290  0.7931459392776503  0.3812416725399572
  0.3845387774080322  0.3197370462956570  0.2953037364850459
  0.8226226714451030  0.2789341572088304  0.3787278164043499
  0.3608888234324610  0.7681510044017017  0.3564809386145953
  0.8894043361646098  0.8178068817934872  0.3981138380239813
  0.3879089933644195  0.5321486538029845  0.3431933722322853
```

0.9102418924251765	0.5688622428630339	0.4386265859063556
0.3442591579581133	0.0847534435989559	0.3764262578912394
0.8660991233074142	0.0425410107333803	0.3879602993380260
0.9297878898075780	0.2170347633508243	0.3902738164467934
0.4480135602783974	0.2161909042853765	0.3021073535185863
0.9842953078063630	0.7359732307491740	0.3970178799065849
0.4616986250360497	0.6981519851276872	0.3688342631319728
0.2237305030833454	0.4000170750762990	0.3470374896722035
0.7274224813341448	0.4368086401517601	0.3070458134872069
0.2698304883594176	0.9280516100622265	0.3244241262037306
0.7060817421518877	0.9520646325622550	0.3748364810349827
0.2287245567699472	0.2650665705039970	0.3081797483024431
0.6669972897034953	0.1868652686735999	0.3662232887417076
0.2052899059877120	0.6892458060178370	0.3982303096633544
0.7274202389790076	0.7188305082171595	0.3990350332525239
0.4803790181174890	0.4810343318465513	0.3017210617879300
0.8697376111478974	0.4446739019526191	0.3515661757891664
0.4026586566561647	0.9041100787676797	0.3046989809413745
0.9663075560343870	0.9807010257343833	0.3969690546080500
0.1020739829004498	0.3876156556340717	0.5272655872399241
0.8898169721979770	0.5487042429571645	0.5424098213304021
0.3304336834705168	0.1151656473778999	0.4770028562394941
0.2159949507008960	0.4795401107684683	0.5474484586536761
0.8397632349928728	0.4298033295742556	0.5663346594604022
0.2516969988519193	0.0144780883135809	0.5218287427206576

REFERENCES

1. Hartmann, M.; Vinu, A. Mechanical Stability and Porosity Analysis of Large-Pore SBA-15 Mesoporous Molecular Sieves by Mercury Porosimetry and Organics Adsorption. *Langmuir* **2002**, *18*, 8010-8016.
2. Kruk, M.; Jaroniec, M.; Sakamoto, Y.; Terasaki, O.; Ryoo, R.; Ko, C. H. Determination of Pore Size and Pore Wall Structure of MCM-41 by Using Nitrogen Adsorption, Transmission Electron Microscopy, and X-ray Diffraction. *J. Phys. Chem. B* **2000**, *104*, 292-301.
3. Li, X. -H.; Wang, X.; Antonietti, M. Mesoporous g-C_3N_4nanorods as multifunctional supports of ultrafine metal nanoparticles: hydrogen generation from water and reduction of nitrophenol with tandem catalysis in one step. *Chem. Sci.* **2012**, *3*, 2170–2174.
4. Liu, J.; Huang, J.; Zhou, H.; Antonietti, M. Uniform Graphitic Carbon Nitride Nanorod for Efficient Photocatalytic Hydrogen Evolution and Sustained Photoenzymatic Catalysis. *ACS Appl. Mater. Interfaces* **2014**, *6*, 8434−8440.

5. Tong, Z.; Yang, D.; Sun, Y.; Nan, Y.; Jiang, Z. Tubular g-C_3N_4 Isotype Heterojunction: Enhanced Visible-Light Photocatalytic Activity through Cooperative Manipulation of Oriented Electron and Hole Transfer. *Small* **2016**, *12*, 4093-4101.
6. Fan, Q.; Liu, J.; Yu, Y.; Zuo, S. A template induced method to synthesize nanoporous graphitic carbon nitride with enhanced photocatalytic activity under visible light. *RSC Adv.* **2014**,*4*, 61877-61883.
7. Jun, Y.-S.; Hong, W. H.; Antonietti, M.; Thomas, A. Mesoporous, 2D Hexagonal Carbon Nitride and Titanium Nitride/Carbon Composites. *Adv. Mater.* **2009**, *21*, 4270-4274.
8. Talapaneni, S. N.; Mane, G. P.; Mano, A.; Anand, C.; Dhawale, D. S.; Mori, T.; Vinu, A. Synthesis of Nitrogen-Rich Mesoporous Carbon Nitride with Tunable Pores, Band Gaps and Nitrogen Content from a Single Aminoguanidine Precursor. *ChemSusChem* **2012**, *5*, 700-708.
9. Fang, Z.; Hong, Y.; Li, D.; Luo, B.; Mao, B.; Shi, W. One-Step Nickel Foam Assisted Synthesis of Holey g-Carbon Nitride Nanosheets for Efficient Visible-Light Photocatalytic H_2 Evolution. *ACS Appl. Mater. Interfaces* **2018**, *10*, 20521-20529.
10. Xing, W.; Tu, W.; Han, Z.; Hu, Y.; Meng, Q.; Chen, G. Template-Induced High-Crystalline g-C_3N_4 Nanosheets for Enhanced Photocatalytic H_2 Evolution. *ACS Energy Lett.* **2018**, *3*, 514-519.
11. Han, Q.; Wang, B.; Gao, J.; Cheng, Z.; Zhao, Y.; Zhang, Z.; Qu, L. Atomically Thin Mesoporous Nanomesh of Graphitic C_3N_4 for High-Efficiency Photocatalytic Hydrogen Evolution. *ACS Nano* **2016**, *10*, 2745-2751.
12. Liu, M.; Xia, P.; Zhang, L.; Cheng, B.; Yu, J. Enhanced Photocatalytic H_2-Production Activity of g-C_3N_4 Nanosheets via Optimal Photo-deposition of Pt as Cocatalyst. *ACS Sus. Chem. Eng.* **2018**, *6*, 10472-10480.
13. Han, Q.; Cheng, Z.; Wang, B.; Zhang, H.; Qu, L. Significant Enhancement of Visible-Light-Driven Hydrogen Evolution by Structure Regulation of Carbon Nitrides. *ACS Nano* **2018**, *12*, 5221-5227.
14. Talapaneni, S. N.; Mane, G. P.; Park, D.-H.; Lakhi, K. S.; Ramadass, K.; Joseph, S.; Skinner, W. M.; Ravon, U.; Al-Bahily, K.;Vinu, A. Diaminotetrazine based mesoporous C_3N_6 with a well-ordered 3D cubic structure and its excellent photocatalytic performance for hydrogen evolution. *J. Mater. Chem. A* **2017**, *5*, 18183-18192.
15. Sun, S.; Gou, X.; Tao, S.; Cui, J.; Li, J.; Yang, Q.; Liang, S.; Yang, Z. Mesoporous graphitic carbon nitride (g-C_3N_4) nanosheets synthesized from carbonated beverage-reformed commercial melamine for enhanced photocatalytic hydrogen evolution. *Mater. Chem. Front.* **2019**, *3*, 597-605.
16. Dong, H.; Xiao, M.; Yu, S.; Wu, H.; Wang, Y.; Sun, J.; Chen, G.; Li, C. Insight into the Activity and Stability of Rh_xP Nano-Species Supported on g-C_3N_4 for Photocatalytic H_2 Production. *ACS Catal.* **2020**, *10*, 458-462.
17. Wang, X.; Zhou, C.; Shi, R; Liu, Q.; Waterhouse, G. I. N.; Wu, L.; Tung, C.-H.; Zhang, T. Supramolecular precursor strategy for the synthesis of holey graphitic carbon nitride nanotubes with enhanced photocatalytic hydrogen evolution performance. *Nano Res.* **2019**, *12*, 2385–2389.

18. Zhang, L.; Ding, N.; Lou, L.; Iwasaki, K.; Wu, H.; Luo, Y.; Li, D.; Nakata, K.; Fujishima, A.; Meng, Q. Localized Surface Plasmon Resonance Enhanced Photocatalytic Hydrogen Evolution via Pt@Au NRs/C_3N_4 Nanotubes under Visible-Light Irradiation. *Adv. Funct. Mater.* **2019**, *29*, 1806774.
19. Jia, J.; Zhang, Q.; Li, Z.; Hu, X.; Liu, E.; Fan, J. Lateral heterojunctions within ultrathin FeS–$FeSe_2$ nanosheet semiconductors for photocatalytic hydrogen evolution. *J. Mater. Chem. A* **2019**, *7*, 3828-3841.
20. Yang, H.; Zhou, Y.; Wang, Y.; Hu, S.; Wang, B.; Liao, Q.; Li, H.; Bao, J.; Ge, G.; Jia, S. Three-dimensional flower-like phosphorus-doped g-C_3N_4 with a high surface area for visible-light photocatalytic hydrogen evolution. *J. Mater. Chem. A* **2018**, *6*, 16485-16494.
21. Wen, P.; Zhao, K.; Li, H.; Li, J.; Li, J.; Ma, Q.; Geyer, S. M.; Jiang, L.; Qiu, Y. *In situ* decorated Ni_2P nanocrystal co-catalysts on g-C_3N_4 for efficient and stable photocatalytic hydrogen evolution *via* a facile co-heating method. *J. Mater. Chem. A* **2020**, *8*, 2995-3004.
22. Liu, J.; Xu, H.; Yan, J.; Huang, J.; Song, Y.; Deng, J.; Wu, J.; Ding, C.; Wu, X.; Yuan, S.; Li, H. Efficient photocatalytic hydrogen evolution mediated by defect-rich 1T-PtS_2 atomic layer nanosheet modified mesoporous graphitic carbon nitride. *J. Mater. Chem. A* **2019**, *7*, 18906-18914.
23. Mane, G. P.; Talapaneni, S. N.; Lakhi, K. S.; lbeygi, H.; Ravon, U.; Al- Bahily, K.; Mori, T.; Park, D.-H.; Vinu, A. Highly Ordered Nitrogen-Rich Mesoporous Carbon Nitrides and Their Superior Performance for Sensing and Photocatalytic Hydrogen Generation. *Angew. Chem. Int. Ed.* **2017**, *56*, 8481-8485.
24. Li, Z.; Wang, X.; Tian, W.; Meng, A.; Yang, L. CoNi Bimetal Cocatalyst Modifying a Hierarchical $ZnIn_2S_4$ Nanosheet-Based Microsphere Noble-Metal-Free Photocatalyst for Efficient Visible-Light-Driven Photocatalytic Hydrogen Production. *ACS Sustainable Chem. Eng.* **2019**, *7*, 20190-20201.
25. Liu, Y.; Xiang, Z. Fully Conjugated Covalent Organic Polymer with Carbon-Encapsulated Ni_2P for Highly Sustained Photocatalytic H_2 Production from Seawater. *ACS Appl. Mater. Interfaces* **2019**, *11*, 41313-41320.
26. Zhou, X.; Zhu, Y.; Gao, Q.; Zhang, S.; Ge, C.; Yang, S.; Zhong, X.; Fang, Y. Modified Graphitic Carbon Nitride Nanosheets for Efficient Photocatalytic Hydrogen Evolution. *ChemSusChem* **2019**, *12*, 4996-5006.
27. Jin, X.; Wang, R.; Zhang, L.; Si, R.; Shen, M.; Wang, M.; Tian, J.; Shi, J. Electron Configuration Modulation of Nickel Single Atoms for Elevated Photocatalytic Hydrogen Evolution. *Angew. Chem.* **2020**, *132*, 6894-6898.
28. Huang, S.; Zhang, Y.; Du, C.; Su, Y. Double defective group modified nitrogen-deficient carbon nitride with bimetallic PtSn as a cocatalyst for efficient photocatalytic hydrogen evolution up to 765 nm. *Chem. Commun.* **2020**, Advance Article.
29. Liu, X.; Jing, B.; Lun, G.; Wang, Y.; Wang, X.; Fang, C.; Ao, Z.; Li, C. Integrating nitrogen vacancies into crystalline graphitic carbon nitride for enhanced photocatalytic hydrogen production. *Chem. Commun.* **2020**, *56*, 3179-3182.

30. Lin, B.; An, H.; Yan, X.; Zhang, T.; Wei, J.; Yang, G. Fish-Scale Structured g-C_3N_4 Nanosheet with Unusual Spatial Electron Transfer Property for High-Efficiency Photocatalytic Hydrogen Evolution. *Appl. Catal. B- Environ.* **2017**, *210*, 173-183.
31. Chen, Y.; Lin, B.; Wang, H.; Yang, Y.; Zhu, H.; Yu, W.; Basset, J.M. Surface Modification of g-C_3N_4 by Hydrazine: Simple Way for Noble-Metal Free Hydrogen Evolution Catalysts. *Chem. Eng. J.* **2016**, *286*, 339-346.
32. Jing, H.; You, M.; Yi, S.; Li, T.; Ji, H.; Wang, Y.; Zhang, Z.; Zhang, R.; Chen, D.; Yang, H. Precursor- Engineering Coupled Microwave Molten- Salt Strategy Enhances Photocatalytic Hydrogen Evolution Performance of g- C_3N_4 Nanostructures. *ChemSusChem.* **2020**, *13*, 827-837.
33. Liang, Q.; Li, Z.; Huang, Z. H.; Kang, F.; Yang, Q. H. Holey Graphitic Carbon Nitride Nanosheets with Carbon Vacancies for Highly Improved Photocatalytic Hydrogen Production. *Adv. Funct. Mater.* **2015**, *25*, 6885-6892.
34. Lin, B.; Yang, G.; Wang, L. Stacking-Layer-Number Dependence of Water Adsorption in 3D Ordered Close-Packed g-C_3N4 Nanosphere Arrays for Photocatalytic Hydrogen Evolution. *Angew. Chem. Int. Ed.* **2019**, *58*, 4587-4591.
35. Martha, S.; Nashim, A.; Parida, K. M. Facile Synthesis of Highly Active g-C_3N_4 for Efficient Hydrogen Production under Visible Light. *J. Mater. Chem. A* **2013**, *1*, 7816.
36. Chen, Y.; Lin, B.; Yu, W.; Yang, Y.; Bashir, S. M.; Wang, H.; Takanabe, K.; Idriss, H.; Basset, J. M. Surface Functionalization of g-C_3N_4: Molecular-Level Design of Noble-Metal-Free Hydrogen Evolution Photocatalysts. *Chem. Euro. J.* **2015**, *21*, 10290-10295.
37. Jiang, Y.; Sun, Z.; Tang, C.; Zhou, Y.; Zeng, L.; Huang, L. Enhancement of Photocatalytic Hydrogen Evolution Activity of Porous Oxygen Doped g-C_3N_4 With Nitrogen Defects Induced by Changing Electron Transition. *Appl. Catal. B- Environ.* **2019**, *240*, 30-38.
38. Li, Y.; Yang, M.; Xing, Y.; Liu, X.; Yang, Y.; Wang, X.; Song, S. Preparation of Carbon-Rich g-C_3N_4 Nanosheets with Enhanced Visible Light Utilization for Efficient Photocatalytic Hydrogen Production. *Small* **2017**, *13*, 1701552.
39. Pawar, R.; Kang, S.; Park, J.; Kim, J.; Ahn, S.; Lee, C. Room-Temperature Synthesis of Nanoporous 1D Microrods of Graphitic Carbon Nitride (g-C_3N_4) with Highly Enhanced Photocatalytic Activity and Stability. *Sci. Rep.* **2016**, *6*.

***